

# Identification of Resonant Frequencies in LIGO-like Suspension with Finite-Element Modeling

Orion Sauter,<sup>\*</sup> Ninad Bhagwat,<sup>†</sup> John Conklin,<sup>‡</sup> and D.B. Tanner<sup>§</sup>

*University of Florida*

(Dated: June 27, 2023)

Following the upgrades to Advanced LIGO (aLIGO), measurements were made of the detector suspensions' frequency response characteristics. While most resonant frequencies could be identified with simple mechanical models, such as the fiber vibration modes, some were unexplained. Using a finite element model of the quadruple pendulum suspension, we search for and identify these frequencies. By modeling these response frequencies we can suggest methods to reduce their amplitude, alter their frequency, or eliminate them in future gravitational wave detector designs.

## I. INTRODUCTION

The aLIGO detectors were designed to detect gravitational waves (GWs) with frequencies in the range 10 Hz to 7000 Hz [1]. The detectors use a Fabry-Perot interferometer to measure the change in differential arm length created by passing gravitational waves. However, the length changes induced by these waves are  $O(10^{-21})$  in strain, and can easily be covered by noise. To achieve the necessary stability, the detectors' suspensions use quadruple pendulums to suspend the test masses, which serve as the end mirrors for the interferometer [2, 3]. Some noise sources are transient, and the affected time spans can be vetoed without much reduction in SNR [4]. However, more persistent noise sources affecting a small range of frequencies, such as mechanical resonances and electrical coupling, can degrade the performance of both stochastic gravitational-wave background (SGWB) and continuous wave (CW) searches when the signal frequency passes through the frequency of the disturbed band. When the noise spectrum is plotted on a semilog scale over many decades, these noise bands appear as single vertical lines; hence, we call them "lines." By identifying and resolving these noise sources, we can improve our detection capabilities. Due to the complexity of the detectors, it is not always clear what causes a given spectral line in the strain sensitivity. If we can find a similar line in a simplified surrogate model, we may be able to identify the source.

Finite-element analysis (FEA) offers a high-fidelity simulation with full knowledge of all components' degree of freedoms (DoFs), including internal models of mechanical components. As an initial target, we choose the aLIGO quadruple pendulum suspensions. These consist of 4 stages: the top (TOP) mass weighing 20 kg supported by two 45 cm long steel wires that are connected to ground by maraging steel blade springs, the upper intermediate mass (UIM) weighing 20 kg supported by four

31 cm long steel wires that are connected to the TOP by blade springs, the penultimate mass (PUM) weighing 40 kg supported by four 34 cm long steel wires that are connected to the UIM by blade springs, and the test mass (TM) weighing 40 kg connected to the PUM by 65 cm direct silica fiber link [3]. Each stage can be measured in the six DoFs, and with the exception of the TM, can be actuated in these DoFs as well.

In Section II we outline the problem of spectral lines. Section III describes the model we used to simulate the detector, and Section IV outlines the conversion from the FEA outputs to a 6 DoF system used to describe the suspensions. Sections V, VI, and VII compare that output to LIGO Hanford Observatory (LHO) measurements via a transfer function.

## II. UNKNOWN SPECTRAL LINES

The Seismic & Suspensions Working Group of the LIGO Scientific Collaboration (SWG) maintains state-space models (SSMs) of the aLIGO pendulums for simulation and testing [5]. These models are each comprised of four matrices which define the time evolution from inputs – applied forces and torques – to outputs – displacements and rotations:

$$\dot{\mathbf{x}} = \mathbf{A}\mathbf{x} + \mathbf{B}\mathbf{u} \quad (1)$$

$$\mathbf{y} = \mathbf{C}\mathbf{x} + \mathbf{D}\mathbf{u} \quad (2)$$

where  $\mathbf{u}$  are inputs,  $\mathbf{y}$  outputs, and  $\mathbf{x}$  states of the system. For second-order systems, the states often represent a series of positions, followed by a series of corresponding velocities. This results in the matrices having a block form, as in the initial version of the SSM, based on a theoretical model of the pendulum, which used rigid body masses, and linearized springs. In this case, the state variables corresponded directly to the six DoFs of each of the stages. However, this model was found to be a poor match to the detector's true behavior. In light of this, the SWG developed a SSM based on measurements of the suspensions, which has a far more complicated structure. Summaries of the theoretical and empirical SSMs are shown in Figures 1 and 2 respectively. After the second aLIGO observing run (O2) measurements

<sup>\*</sup> orionsauter@ufl.edu

<sup>†</sup> ninadgbhagwat@gmail.com

<sup>‡</sup> jwconklin@ufl.edu

<sup>§</sup> tanner@phys.ufl.edu

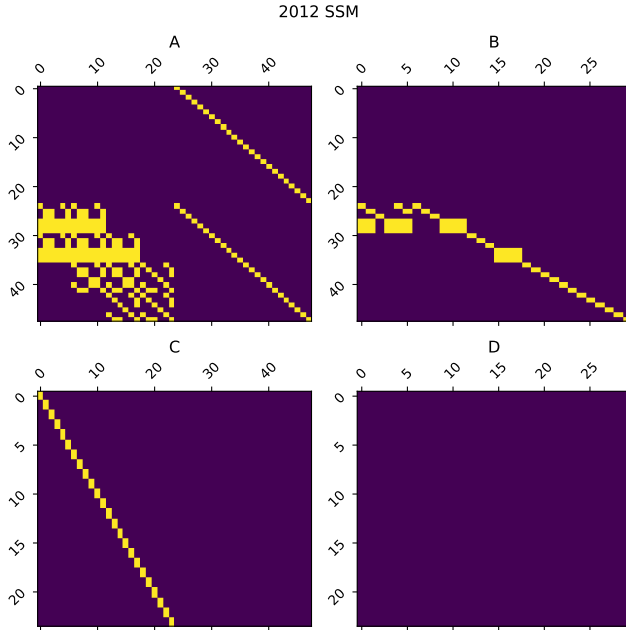


FIG. 1. Non-zero elements (yellow) of component matrices of theoretical SSM from 2012.

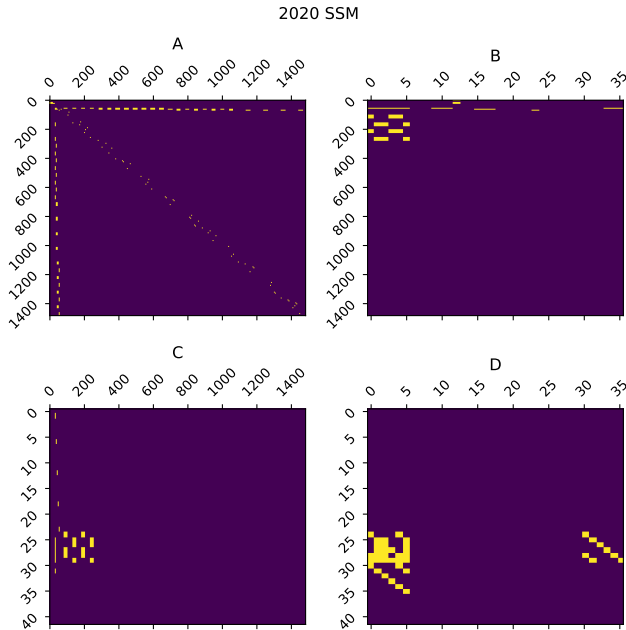


FIG. 2. Non-zero elements (yellow) of component matrices of empirical SSM from 2020.

were made of narrow spectral lines in the detectors [6]. By using physical environment monitors (PEMs), we can identify lines due to local disturbances [7]. Other lines can be attributed to known mechanical features, such as the vibrational modes of the suspensions [8]. However, some lines could not be identified. Without knowing the sources of these lines, we have no way suppress or alter

them.

### III. FINITE-ELEMENT MODEL

FEA is a common technique in engineering and design to analyze the stresses within a large structure under applied forces. The University of Glasgow has developed a finite-element model of the aLIGO quadruple pendulums using the ANSYS software package [9]. They used this model to analyze the modes of the blade springs that support the weight of the test masses (Figure 4). However, for our analysis, we wish to consider the stages of the pendulum as units, rather than the individual components.

Although the motion of the stages is driven by eigenmodes calculated from modal analysis, motion response is better calculated with transient time series analysis. In this method a non-periodic, non-harmonic time dependent external load is applied to the structure and the resultant displacement, strain, stress, and reaction forces are computed using the following governing equation:

$$M\ddot{\mathbf{u}}(t) + C\dot{\mathbf{u}}(t) + K\mathbf{u}(t) = \mathbf{F}(t), \quad (3)$$

where  $M$  is the mass matrix,  $C$  is the damping matrix,  $K$  is the stiffness matrix,  $F(t)$  is the applied load, and  $\mathbf{u}(t)$  is the nodal displacement.

There are various finite element methods to solve the above governing equation. Among these are the full method, Mode Superposition (MSUP) method etc. The MSUP method first computes the mode shapes using modal analysis and then combines them to obtain the higher frequency modes. The MSUP method is faster and more efficient but only supports linearity. The full method uses the whole matrices to calculate the dynamic behavior of the system. Unlike the MSUP method, the full method supports non-linearity and produces accurate results for large displacements. Since nonlinear effects are involved in our model, we have used the full method.

Unfortunately, this introduces further complications, as we must apply gravity to have a restoring force, and the flat springs used in the Glasgow model are not able to support the 40 kg masses that make up the lowest two stages. In the physical system, the blades are pre-stressed with an upward curvature which induces compressive residual stress at the top surface and tensile residual stress at the bottom surface. When the blades are loaded with the test masses, the prestress is balanced by the weight acting downward due to gravity. At equilibrium, weight is equal to the prestress and the blades become flat. By simulating these blade springs in isolation, we can generate the induced stresses from the bending force, then import them onto the flat springs in the full model.

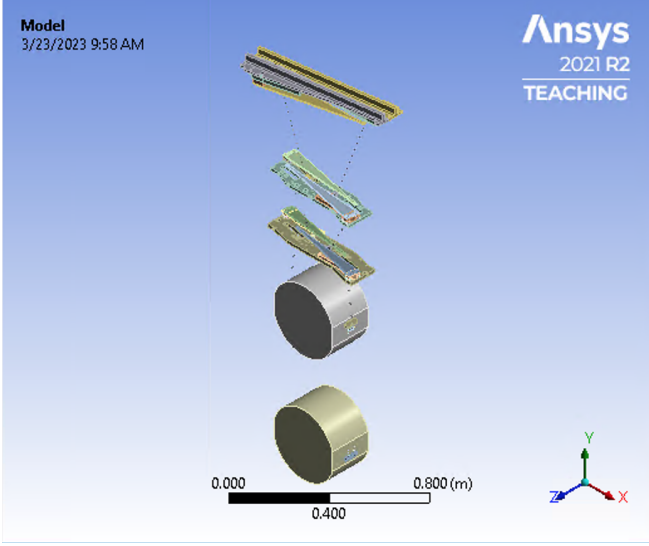


FIG. 3. University of Glasgow finite-element model of the aLIGO quadruple pendulum.

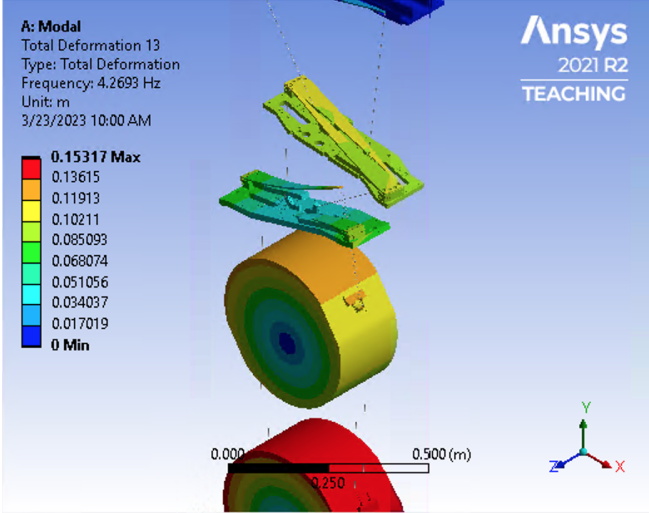


FIG. 4. Bending mode of blade springs.

#### IV. SIX DEGREE OF FREEDOM AGGREGATION

For simplicity, the position of each stage is typically expressed in terms of longitudinal, vertical, and transverse displacements, and roll, yaw, and pitch angles. In Figure 3, these correspond to displacements and rotations in  $z$ ,  $y$ , and  $x$ , respectively. However, the ANSYS results contain information for the individual nodes that make up the model. To convert these, for each component we find the centroid  $\mathbf{c}$ , and then for each node the relative position  $\mathbf{r} = \mathbf{p} - \mathbf{c}$ . Each node has an initial position expressed as a vector from the origin,  $\mathbf{p}^{\text{loc}}$ , and a displacement expressed as a vector from the initial position,  $\mathbf{p}^{\text{disp}}$ . Using these properties, we can define the six

DoFs, which we average over the component's nodes:

$$L = p_z^{\text{disp}} \quad (4)$$

$$V = p_y^{\text{disp}} \quad (5)$$

$$T = p_x^{\text{disp}} \quad (6)$$

$$R = \frac{1}{2} (\arctan(p_y^{\text{disp}}/r_z^{\text{loc}}) + \arctan(p_z^{\text{disp}}/r_y^{\text{loc}})) \quad (7)$$

$$Y = \frac{1}{2} (\arctan(p_x^{\text{disp}}/r_z^{\text{loc}}) + \arctan(p_z^{\text{disp}}/r_x^{\text{loc}})) \quad (8)$$

$$P = \frac{1}{2} (\arctan(p_y^{\text{disp}}/r_x^{\text{loc}}) + \arctan(p_x^{\text{disp}}/r_y^{\text{loc}})) \quad (9)$$

#### V. TRANSFER FUNCTION ESTIMATION

The measurements made by the aLIGO SWG are in the form of transfer functions relating applied forces and torques to displacements and rotations for the DoFs of the stages of the pendulum. For comparison, we need to generate similar transfer functions for our model.

For a given input stage and DoF, we apply Gaussian noise as a force with a 1 kHz sampling rate in a transient analysis. We then measure the 6 DoF displacement of the stages in time, and take the desired output DoF. The estimated transfer function is then the Fourier transform of the output divided by the Fourier transform of the input.

#### VI. CASE STUDY: 166 HZ LINE

Among the unidentified spectral lines found following O2 was one at approximately 166 Hz, in the transfer function between the longitudinal DoFs of the UIM and TM. Despite efforts by the SWG, the source of this line could not be found. We chose this as a target study for the use of our model. Using the technique described above, we estimated the transfer function for this coupling in the ANSYS model, and show a comparison to measurements of LHO in Figure 5.

While the ANSYS model gives a slightly higher frequency of 174.5 Hz, this is not far off from the measured 166.375 Hz. The Q factors, found from estimates of the full-width at half-maximum of the curves shown in Figure 5, are also similar with 30.9 for ANSYS vs. 40.6 measured.

Assuming these peaks result from similar motion of the pendulum, we can use ANSYS to determine what components are responsible for the behavior. If we drive the UIM stage at 174.5 Hz, and measure the vertical displacement for points across the transverse axis of the UIM, we see a rocking motion shown in Figure 6. However, this motion is more commonly seen at low frequency, due to the off-center positioning of the blade springs. By looking at the strain distribution over the components of the UIM in Figure 7, we see there is significant energy in the connection points between the blade springs and the base plate. We can bandpass the motion in the range 150 Hz to 200 Hz, and look at the vertical deformation over the surface of the UIM base plate (Figure 8).

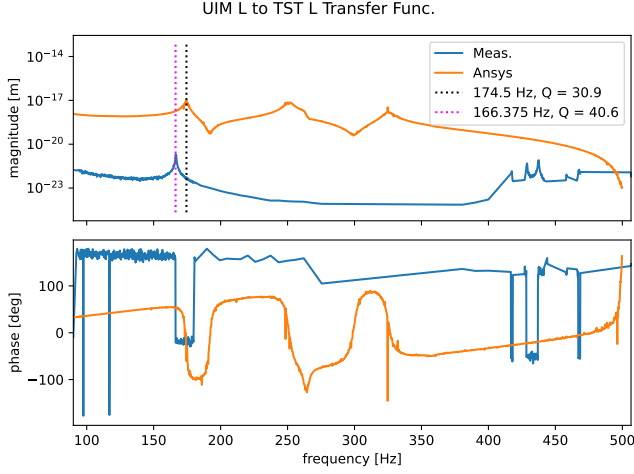


FIG. 5. Transfer function between UIM and TM longitudinal DoFs.

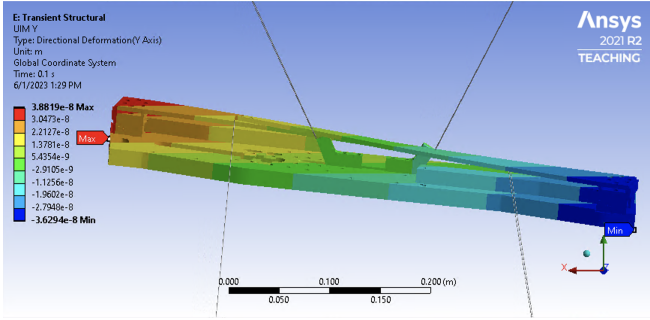


FIG. 6. Vertical motion of UIM base plate under 174.5 Hz longitudinal force.

The two regions of high-deformation in Figure 8 correspond to the blocks connecting the blade springs to the base plate. We show the time-evolution of these two areas in Figure 9. This shows the two connection points vibrating in opposite directions at the frequency measured in the transfer functions. Reinforcing the base plate in the regions where the blade springs connect may help to reduce this motion and increase the frequency.

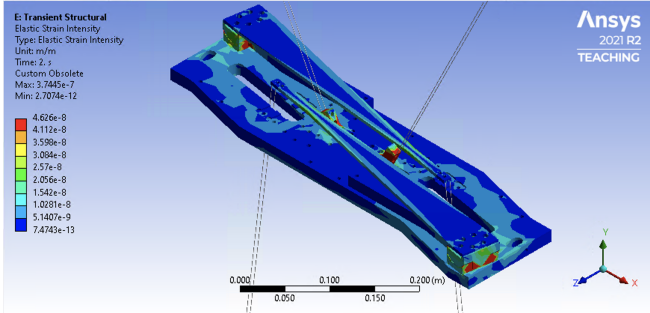


FIG. 7. Measured elastic strain in UIM under 174.5 Hz excitation.

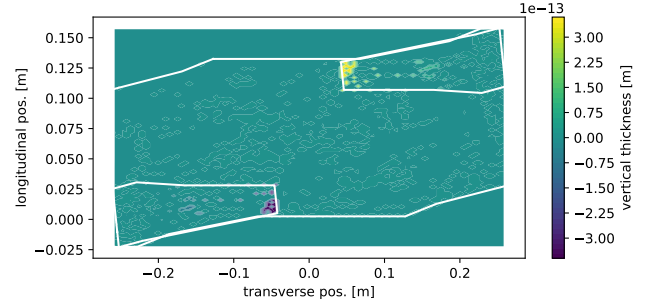


FIG. 8. Change in UIM base plate thickness under force. White lines show the outlines of the base plate, and spring supports. The apparent discontinuities are due to the resolution of the simulation. However, these differences are small, and it is through the stiffness of the material that they are able to have a measurable effect.

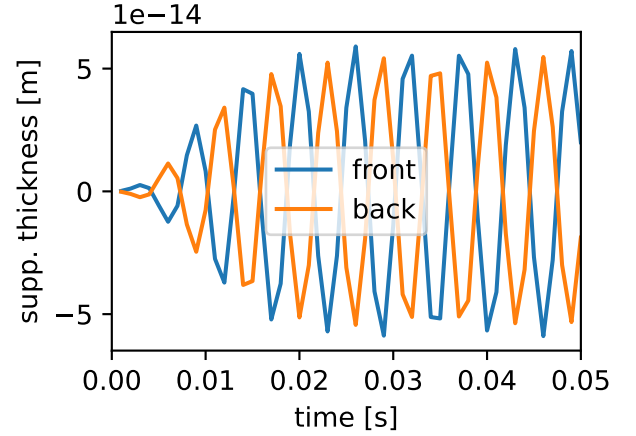


FIG. 9. Vertical deformation in time for blade spring connection pads.

## VII. CASE STUDY: 431 HZ LINE

Looking at differences in response between the two SSMs discussed above, we found a line in the UIM vertical to TM longitudinal transfer function at 431.34 Hz (Figure 10). As above, we can examine the motion of the ANSYS model at this frequency when driven in the vertical direction. Again we see distortions in the areas of the UIM base plate under the spring supports, though in this case the motion between front and back is in-phase (Figure 11). The measured thickness of the UIM base plate shows a similar pole/zero combination to the SSM, though again at a lower frequency (Figure 12).

As with the first line investigated, this one appears to be the result of distortions to the UIM directly under the supports holding the PUM and TM. Planned next-generation detectors such as Cosmic Explorer [10] and Einstein Telescope [11] will use similar suspensions with larger masses, potentially increasing the stresses induced

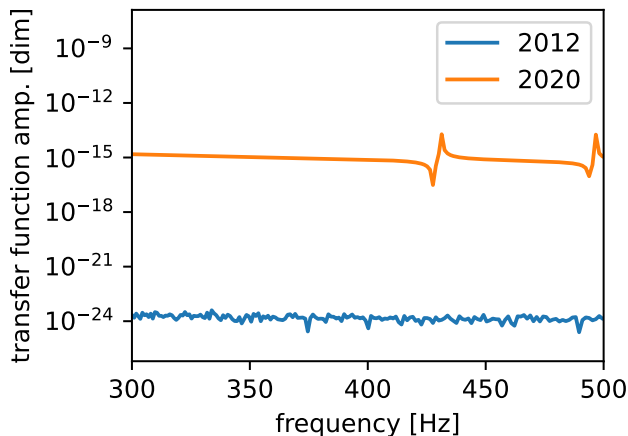


FIG. 10. UIM vertical-to-TM longitudinal transfer functions for 2012 and 2020 SSMs.

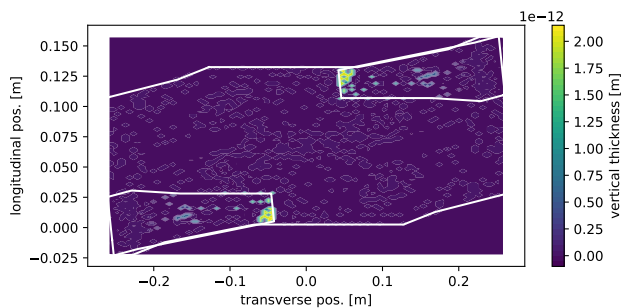


FIG. 11. Change in UIM base plate thickness under force. White lines show the outlines of the base plate, and spring supports.

on the upper stages, and so effects like these should be taken into account.

## VIII. CONCLUSIONS

Any future GW detector is likely to exhibit unintended mechanical modes in the suspension system that generate spectral lines in the strain sensitivity. By modeling the design in FEA, we may be able to foresee these lines, and either shift them to a less valuable frequency or reduce them significantly. While SSMs are useful for simulating the behavior of a particular suspension, using FEA can inform the reasons for that behavior. Models like the one shown here can illustrate internal modes, and identify cross-couplings. With this more detailed but still virtual view of the suspensions, we can assess the model for unexpected noise sources, and resolve them before finalizing and fabricating the design.

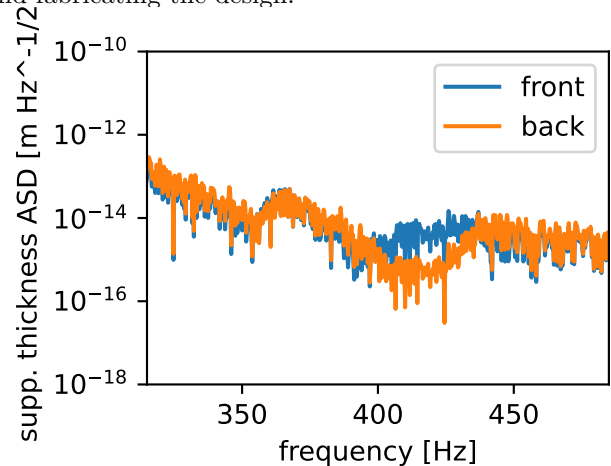


FIG. 12. UIM thickness under vertical displacement.

## ACKNOWLEDGMENTS

The authors thank Giles Hammond, Alan Cumming, and Graeme Eddolls at the University of Glasgow for the use of their pendulum model.

This material is based upon work supported by the National Science Foundation under Grant No. PHY-2012021.

- 
- [1] J. Aasi *et al.* (The LIGO Scientific Collaboration), Advanced LIGO, Classical and Quantum Gravity **32**, 074001 (2015).
  - [2] N. A. Robertson *et al.*, Quadruple suspension design for advanced ligo, Classical and Quantum Gravity **19**, 4043 (2002).
  - [3] S. M. Aston *et al.*, Update on quadruple suspension design for advanced ligo, Classical and Quantum Gravity **29**, 235004 (2012).
  - [4] B. P. Abbott *et al.*, Effects of data quality vetoes on a search for compact binary coalescences in advanced ligo's first observing run, Classical and Quantum Gravity **35**, 065010 (2018).
  - [5] M. Barton, C. Torrie, K. Strain, and N. Robertson, *Models of the Advanced LIGO Suspensions in MATLAB*, Tech. Rep. LIGO-T080188 (LIGO Laboratory, 2012).
  - [6] P. B. Covas *et al.* (LSC Instrument Authors), Identification and mitigation of narrow spectral artifacts that degrade searches for persistent gravitational waves in the first two observing runs of advanced ligo, Phys. Rev. D **97**, 082002 (2018).
  - [7] A. Effler, R. M. S. Schofield, V. V. Frolov, G. González, K. Kawabe, J. R. Smith, J. Birch, and R. McCarthy, Environmental influences on the ligo gravitational wave

- detectors during the 6th science run, *Classical and Quantum Gravity* **32**, 035017 (2015).
- [8] D. V. Martynov *et al.*, Sensitivity of the advanced ligo detectors at the beginning of gravitational wave astronomy, *Phys. Rev. D* **93**, 112004 (2016).
  - [9] L. Cunningham, G. Hammond, K. Strain, C. Torrie, and N. Robertson, *Estimate of thermal and seismic noise from aLIGO quad suspension blade springs*, Tech. Rep. LIGO-T1300595-v1 (University of Glasgow, 2014).
  - [10] M. Evans *et al.*, A Horizon Study for Cosmic Explorer: Science, Observatories, and Community, (2021), arXiv:2109.09882 [astro-ph.IM].
  - [11] S. Di Pace *et al.*, Research facilities for europe’s next generation gravitational-wave detector einstein telescope, *Galaxies* **10**, 10.3390/galaxies10030065 (2022).
  - [12] B. P. Abbott *et al.*, A guide to ligo–virgo detector noise and extraction of transient gravitational-wave signals, *Classical and Quantum Gravity* **37**, 055002 (2020).